Optica Applicata, Vol. XIX, No. 3, 1989

Simulation of anticipated operation characteristics of designed constructions of broad-contact double-heterostructure (AlGa)As diode lasers. III. Quantum efficiencies and the thermal properties*

W. Nakwaski

Institute of Physics, Technical University of Łódź, ul. Wólczańska 219, 93–005 Łódź, Poland.

In this work, the third part of the model of broad-contact double-heterostructure (AlGa)As diode lasers is presented. The formulae given in this part enable us to determine the quantum efficiencies of the laser and the temperature increases within it .

1. Introduction

In two previous parts of the model of broad-contact double-heterostructure (AlGa)As diode lasers we have presented the formulae necessary for determining a threshold current and a coefficient of free-carier absorption, respectively. In this part, we shall describe quantum efficiencies and thermal properties of the laser.

2. Internal quantum efficiencies

Internal quantum efficiencies of the spontaneous emission and of the lasing are given by:

$$\eta_{SP} = (1 + t_R/t_{NR})^{-1}, \tag{1}$$

$$\eta_i = \eta_H/(1 + t_R/t_{NR}), \tag{2}$$

respectively, where t_R and t_{NR} are the radiative and the nonradiative minority-carrier lifetimes, and η_H is the coefficient in which the influence of the internally circulating modes is taken into account. These modes produce no light at the laser facet.

3. Radiative lifetime

From the measurements of the radiative liftime t_R in the p-GaAs performed by Casey and Stern [1] and Nelson and Sobers [2], it follows that a double logarithmic plot of t_R versus the hole concentration p is practically a straight line. Therefore the

* This work was carried out under the Polish Central Program for Fundamental Research CPBP 01.06., 6.04.

radiative lifetime in p-GaAs at room temperature may be presented in the following form:

$$t_{R,0} = 10^{-7}(p/10^{16})^{-0.75}, \quad \text{sec} \tag{3}$$

where p is taken in cm^{-3}.

GARBUZOV et al. [3], [4] have examined the temperature dependence of the minority-carrier lifetime for samples, the total lifetime of which is approximately equal to the radiative lifetime. The results of these measurements allowed us to formulate this dependence in a following form:

$$t_R(T)/tr(300\,K) = (T/300)^{R(x)} \tag{4}$$

where

$$R(x) = 1.58 + 2.5x. \tag{5}$$

The composition dependence of the radiative lifetime may, in turn, be determined from the Fig. 4.6.4. in [5]. In this figure, the fraction of electrons in the direct conduction band in the $Al_xGa_{1-x}As$ material is shown as a function of its composition. The radiative lifetime t_R, being the inverse of a radiative transition probability P_R, may be written as

$$t_R = P_R^{-1} = (n_\Gamma + n_L + n_X)/n \tag{6}$$

where n_Γ, n_L and n_X are the electron concentrations in the direct Γ and the indirect L and X conduction bands, respectively. The composition dependence of the radiative lifetime in $Al_xGa_{1-x}As$ may be now expressed in the following form:

$$t_R(x)/t_R(0) = 1 + a_x \exp(b_x x) \tag{7}$$

where the a_x and the b_x parameters are listed in Table 1.

Table 1. Values of the a_x and the b_x parameters from Eq. (7)

Parameter	$x \leqslant 0.335$	$x \geqslant 0.335$
a_x	1.019×10^{-3}	7.341×10^{-6}
b_x	22.22	36.92

Taking together all the above relations, we may finally write the radiative lifetime t_R in a following form:

$$t_R(x, T, p)\,[\text{sec}] = 10^{-7}(p[cm^{-3}]/10^{16})^{0.75}(T/300)^{1.58+2.5x}[1 + a_x \exp(b_x x)]. \tag{8}$$

4. Nonradiative lifetime

The nonradiative losses in the active layer may be lumped together in a single effective, nonradiative lifetime t_{NR} [6]

$$t_{NR}^{-1} = (t_{NR,B}) + 2s/d_A \tag{9}$$

where $t_{NR,B}$ is the bulk non radiative lifetime, s is the recombination velocity at the interface of the heterostructure and d_A is the thickness of the active layer.

5. Bulk nonradiative lifetime

For relatively low carrier injection levels, the carrier distribution among the conduction band valleys follows the effective density of states N_C and N_{CX} (c.f. Eq. (31) in the first part of the work). Then the ratio of the radiative lifetime and the bulk nonradiative lifetime may be given by [7], [8]

$$t_R/r_{NR,B} = M(m_{EX}/m_{E\Gamma})^{3/2}\exp(E_{G\Gamma}-E_{GX})/k_B T \tag{10}$$

where k_B is the Boltzmann's constant, T is temperature, M is the number of equivalent indirect valleys (for (AlGa)As, $M = 6$ [9]), $m_{E\Gamma}$ and m_{EX} are the electron effective masses for the conduction bands Γ and X, respectively (see Eqs. (35) and (37) in the first part of the work), and $E_{G\Gamma}$ and E_{GX} are the Γ and X energy gaps (see Eqs. (10) and (34), ibid.).

6. Interface recombination velocity

Kressel et al. [10], [11] have pointed out that the recombination velocity at the heterostructure interface is directly proportional to the relative lattice mismatch at the interface

$$s = 2\times 10^7\,\Delta a/a, \qquad \mathrm{cm/sec} \tag{11}$$

where a is the lattice constant of the active layer material and Δa is the difference in the lattice constants at the heterostructure interface.

Nelson and Sobers [12] have proved that the above proportionality factor is overestimated being determined without taking account of the self-absorption effects. For example, from the measurements published by 't Hooft and van Opdorp [13] it follows that for the LPE $Al_{0.12}Ga_{0.88}As/Al_{0.47}Ga_{0.53}As$ heterostructure s is equal to only 1050 cm/sec at 300 K.

Table 2. Lattice constants a and thermal expansion coefficients α_A of GaAs and AlAs

Material	T [K]	a [Å]	α_A [10^{-6} K^{-1}]
GaAs	300	5.65325 [14], [15]	6.86 [16]
AlAs	273	5.6605 [15], [17]	5.20 [17]

On the basis of the data listed in Table 2, the $Al_xGa_{1-x}As$ lattice constant (in Angstroems) reads as follows

$$a(x,T) = 5.65325\,[1+1.424\times 10^{-3}x+(6.86-1.66x)\,10^{-6}(T-300)], \tag{12}$$

and the difference in the lattice constant (also in Angstroems) may be expressed as

$$\Delta a(x,T) = [8.05\times 10^{-3}-1.66\times 10^{-6}(T-300)]\,\Delta x. \tag{13}$$

Finally, we may write the following relation for s:

$$s = 2.1\times 10^6(\Delta a/a) \quad \mathrm{cm/sec} \tag{14}$$

7. Internally circulating modes

In broad-contact diode lasers, the influence of internally circulating modes on the device efficiency is significant. Unfortunately, we know only results of measurements performed by HENSHALL [18]. Based on these data, the η_H coefficient may be determined as follows

$$\eta_H = 0.67/0.90 = 0.74 \tag{15}$$

8. External differential quantum efficiency

We use the modified version of the expression given in [19] and derived later in [20], i.e.

$$\eta_D = \eta_i/(1+\alpha_i/\alpha_{END}) \tag{16}$$

where α_i and α_{END} are the internal losses and the end losses, respectively (c.f. Eqs. (11) and (13) in the first part of the work). Owing to the operation in the strongly stimulated emission regime, the η_i value in (16) may be higher than that calculated in (2) but it does not exceed the η_H value.

9. Thermal resistances

Let us introduce the following thermal resistances

$$\theta_{T,i} = \Delta T_i/P_T, \quad i = \text{A, P, N, C, T, S} \tag{17}$$

where P_T is the total heat flux generated in a diode laser and ΔT_i is the temperature increase in the centre of the i-th layer. The equivalent thermal model of the considered diode laser is shown in Fig.1.

Layer symbol	Layer number	Thermal conductivity	Function
S	6	λ_G	substrate
T	5	λ_G	transfer
N	4	λ_B	confinement
A	3	λ_A	active
P	2	λ_B	confinement
C	1	λ_G	capping
E	0	λ_G	contact & heat sink

Fig. 1. Simplified thermal model of a broad-contact double-heterostructure (AlGa)As diode laser

10. Thermal resistances of the heat sink and the contact

CARSLAW and JAEGER [21] have shown that for the rectangular ($W\times L$) uniform heat source the mean spreading thermal resistance θ_{HS} of the semi-infinite medium of the thermal conductivity λ_{HS} is of the form

$$\theta_{HS} = (\lambda_{HS} \pi L^2 W^2)^{-1} \{W^2 L \sinh^{-1}(L/W) + W L^2 \sinh^{-1}(W L) + (1/3)[W^3 + L^3 - (W^2 + L^2)^{3/2}] \tag{18}$$

where W and L are the width and the length of the laser crystal.

The thermal resistance of the contact consists of thermal resistances of individual contact layers connected in series, i.e.

$$\theta_{CON} = (1/LW) \sum_i (\delta_i/\lambda_i) \tag{19}$$

where δ_i and λ_i are the thickness and thermal conductivity, respectively, of the i-th contact layer.

The thickness of a thermally equivalent GaAs layer (the E layer, i.e. the layer No. 0 in Fig. 1) the thermal resistance of which is equal to the sum of thermal resistances of laser heat sink and laser contact, is expressed by

$$d_E = LW \lambda_G (\theta_{HS} + \theta_{CON}). \tag{20}$$

11. Temperature increases

The temperature increases in the centres of the individual layer (see subscript) may be written in the following form

$$\Delta T_k = LW \sum_i^6 g_i \, d_i \, \theta_{ki} \qquad \text{for } k = \text{A, N, P, C, S, T} \tag{21}$$

where g_i, d_i and θ_{ki} are listed in Tables 3 and 4.

Table 3. g_i, d_i and θ_{ki} values

i	0	1	2	3	4	5	6
g_i	0	$g_{J,C}+g_{T,C}$	$g_{J,P}$	g_A	$g_{J,N}$	$g_{J,S}+g_{T,T}$	$g_{J,S}$
d_i	d_E	d_C	d_P	d_A	d_N	d_T	d_S
θ_{Ci}	θ_E	θ_C	θ_C	θ_C	θ_C	θ_C	θ_C
θ_{Pi}	θ_E	θ_C	θ_P	θ_P	θ_P	θ_P	θ_P
θ_{Ai}	θ_E	θ_C	θ_P	θ_A	θ_A	θ_A	θ_A
θ_{Ni}	θ_E	θ_C	θ_P	θ_A	θ_A	θ_N	θ_N
θ_{Ti}	θ_E	θ_C	θ_P	θ_A	θ_N	θ_T	θ_T
θ_{Si}	θ_E	θ_C	θ_P	θ_A	θ_N	θ_T	θ_S

Table 4. θ_k values

k	$LW\theta_k$
E	$d_E/2\lambda_G)$
C	$LW\theta_E + (d_E + d_C)/(2\lambda_G)$
P	$LW\theta_C + (d_C/\lambda_G + d_P/\lambda_B)/2$
A	$LW\theta_P + (d_P/\lambda_B + d_A/\lambda_A)/2$
N	$LW\theta_A + (d_A/\lambda_A + d_N/\lambda_N)/2$
T	$LW\theta_N + (d_N/\lambda_N + d_T/\lambda_G)/2$
S	$LW\theta_T + (d_T + d_S)/(2\lambda_G)$

12. Densities of heat sources

In the laser diode the most efficient heat source is placed in the active layer and is connected mainly with nonradiative recombination, and, to some extent, with reabsorption of radiation. Its density of generated power (in W/cm^3) may be expressed in the following way [22]:

$$g_A = (U/d_A)\{j_{TH}(1-\eta_{SP}f_T)+(j-j_{TH})[1-\eta_D-(1-\eta_i)\eta_{SP}]f_T\} \tag{22}$$

where U is the voltage drop at the p-n junction, and j and j_{TH} are the supply and the threshold current densities, respectively. Coefficient f_T describes the fraction of the spontaneous emission from the active layer, transferred radiatively through the wide-gap confinement layers; it may be expressed as follows [23]:

$$f_T = 2\sin^2(\alpha_{CR}/2), \tag{23}$$

with

$$\alpha_{CR} = \arcsin(n_{RB}/n_{RA}) \tag{24}$$

where n_{RB} and n_{RA} are the refractive indices of the confinement layer and of the active layer, respectively (see Eq. (8) in the first part of the model).

The spontaneous radiation transferred through the passive layers is absorbed in the capping layer ($g_{T,C}$) as well as in the lower part (the T layer, i.e., the layer No. 5 in Fig. 1) of the substrate ($g_{T,T}$). The densities of the heat power generated in this process may be expressed in the following way:

$$g_{T,C} = Uj_{TH}\eta_{SP}f_T/2d_C, \tag{25}$$

$$g_{T,T} = Uj_{TH}\eta_{SP}f_T(2d_T). \tag{26}$$

The Joule heating is in each layer generated with the density

$$g_{J,k} = j^2\varrho_k, \quad \text{for } k = \mathrm{C, P, N, S} \tag{27}$$

where ϱ_k is the electrical resistivity of the k-th layer.

13. Electrical resistivities

The electrical resistivity of the k-th layer may be obtained from the relation

$$\varrho_k = (n_k\mu_k e)^{-1} \tag{28}$$

where n_k is the concentration of the carriers, μ_k – their mobility, and e is the unit charge.

14. Mobilities

According to BLAKEMORE [24], the hole mobility in the GaAs material can be expressed in the form

$$\mu_H = [2.5\times10^{-3}(T/300)^{2.3}+A_H10^{-3}(300/T)^{1.5}]^{-1}, \quad \mathrm{cm^2/V\ sec.} \tag{29}$$

Using the results of SZE and IRVIN [25], the A_H coefficient may be determined as

$$A_H = \left.\begin{array}{l} 2.18+0.746\,[\log(p/10^{17})]^{3.357} \\ 2.18+1.585\,[\log(p/10^{17})]^{2.275} \end{array}\right\} \begin{array}{l} \text{for } 4\times10^{17} < p < 10^{19}, \\ \text{for } 10^{19} < p < 10^{20}. \end{array} \tag{30}$$

with p (the hole concentration) in cm^{-3}. The exactness of the above approximation is not worse than 3.5%.

Similar expression is assumed for the electron mobility in GaAs

$$\mu_E = [1.064\times10^{-4}(T/300)^{2.3}+A_E\times10^{-4}(300/T)^{1.5}]^{-1}, \quad [\text{cm}^2/\text{V sec}] \tag{31}$$

where the coefficient A_E has been determined from the results published by STRINGFELLOW [26]

$$A_E = 0.812+0.313\,[\log(n/10^{16})]^{2.35} \tag{32}$$

with n (electron concentration) in cm^{-3}. For n ranging from 5×10^{16} cm^{-3} to 10^{19} cm^{-3}, the exactness of the above approximation is not worse than 3.7%.

The composition dependence of the electron (hole) mobility in the $Al_xGa_{1-x}As$ material may be given by

$$\mu_{E(H)}(x) = \mu_{E(H)}(0)\,B_\mu(x) \tag{33}$$

where the coefficient $B_\mu(x)$ has been determined on the basis of the results published by NEUMANN [27] in the form of the following broken function

$$B_\mu(x) = \left.\begin{array}{l} 1-1.34\,x \\ 1.602-4.39\,x \\ 1.303-3.38\,x \\ 0.33-0.60\,x \\ 0.09 \end{array}\right\} \begin{array}{l} \text{for } x \leqslant 0.19, \\ \text{for } 0.19 < x \leqslant 0.30, \\ \text{for } 0.30 < x \leqslant 0.35, \\ \text{for } 0.35 < x \leqslant 0.40, \\ \text{for } 0.40 < x. \end{array} \tag{34}$$

15. Thermal conductivities

AFROMOWITZ [28] has measured the thermal resistivities of the $Al_xGa_{1-x}As$ material at room temperature for its various compositions. Taking into account these results and the thermal conductivity of the GaAs material measured by MAYCOCK [29], ADACHI [30] has formulated the room temperature dependence of the $Al_xGa_{1-x}As$ thermal conductivity in the following form:

$$\lambda(x) = 100/(2.27+28.83x-30x^2), \quad \text{W/mK}. \tag{35}$$

The temperature dependence of the GaAs thermal conductivity has been determined by AMITH et al. [31] in the the following form:

$$\lambda_G(T) = \lambda_G(300\,\text{K})(300/T)^{1.25}. \tag{36}$$

The same relative temperature dependence is assumed for the $Al_xGa_{1-x}As$ material [32].

16. Beam divergence

The detailed analysis of the mode propagation in symmetric double-heterostructure waveguides allowed BOTEZ and ETTENBERG [33], [34] to formulate the approximate analytical relations for $\theta_{1/2}$, i.e., for the angle at one half of the maximum of the far-field intensity distribution, namely

$$\theta_{1/2} = \left.\begin{array}{ll} 0.65\,D(n_{RA}^2 - n_{RB}^2)^{1/2}/(1+0.086\,uD^2) & \text{for } D \leqslant 1.5, \\ 2\tan^{-1}[(0.59\lambda)/(\pi w_0)], & \text{for } 1.5 < D < 6, \end{array}\right\} \tag{37}$$

with D given by Eq. (7) in the first part of the model and

$$u = \frac{2.52\,(n_{RA}^2 - n_{RB}^2)^{1/2}}{\arctan n\,[0.36(n_{RA}^2 - n_{RB}^2)^{1/2}]} - 5.17, \tag{38}$$

$$w_0 = d_A(0.31 + (3.15/D^{3/2}) + 2/D^6). \tag{39}$$

17. Procedure of the calculations

The flow chart of the self-consistent method for the threshold current determinatioı is shown as an example of the calculations in Fig. 2. The program needs thε following input data:.

i) thicknesses d_i doping p_i or n_i and compositions x_i of all the semiconductor layers,

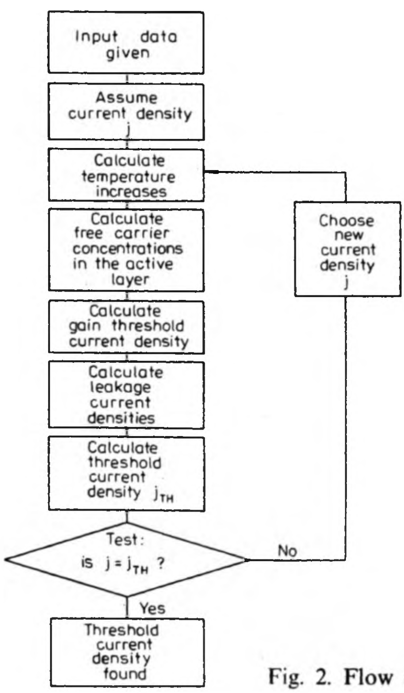

Fig. 2. Flow chart of the threshold-current-density determination

ii) thicknesses δ_i and thermal conductivities λ_i of all the contact and solder layers,

iii) length L and width W of the diode crystal,

iv) ambient temperature T_0,

iv) number N_T length l_T and height h_T of the growth terraces in the cavity.

Typical computer printout of the results of calculations is shown in Table 5. As one can see, for this typical structure of the double-heterostructure GaAs/(AlGa)As diode laser with the active area of dimensions: 400 μm × 100 μm × 0.2 μm, the room-temperature threshold current density for the continuous wave (CW) operation has been determined to be $j_{TH} = 2.09$ kA/cm^2, and the quantum efficiencies of the lasing, i.e., the internal quantum efficiency η_i and the external differential quantum efficiency η_D, are equal to $\eta_i = 63\%$, and $\eta_D = 35\%$.

For similar laser structures, the most respresentative experimental values of the threshold current densities range between 1.5 kA/cm^2 [35] and 2.2 kA/cm^2 [36]. The analogous value for the pulse operation is a little less $j_{TH,P} = 1.35$ kA/cm^2 [37] because in this case the thermal processes become less important. The experimental values of the internal η_i and external differential η_D quantum efficiencies range from 55% [36] to 65% [35], and from 31% [36] to 45% [35], respectively. As one can see, all the theoretical values are inside the given experimental ranges, what confirms the validity of the presented model.

Table 5. Typical printout of the computer calculations

COMPUTER SIMULATION OF SEMICONDUCTOR LASER OPERATION CHARACTERISTICS

INPUT DATA

THICKNESSES AND DOPING OF SEMICONDUCTOR LAYERS ***** SI UNITS

NUMBER	THICKNESS	DOPING	
0	1.466354&-5	GAAS LAYER THERMALLY EQUIVALENT TO THE HEAT - SINK AND THE CONTACT	
1	2.000000&-6	P = 4.00&24	P - GAAS LAYER
2	2.000000&-6	PP = 6.00&24	PP - (ALGA)AS LAYER - XB = 0.300
3	2.000000&-7	PA = 2.00&24	A - (ALGA)AS ACTIVE LAYER - XA = 0.000
4	3.000000&-6	NN = 2.00&24	NN - (ALGA)AS LAYER - XB = 0.300
5	1.000000&-6	N = 2.00&24	TRANSFER N - GAAS LAYER
6	9.180000&-5	N = 2.00&24	N - GAAS SUBSTRATE

DIMENSIONS OF THE DIODE CRYSTAL

LENGTH L = 4.000&-4 WIDTH W = 1.000&-4

AMBIENT TEMPERATURE T0 = 3.000&2

NUMBER, LENGTH AND HEIGHT OF THE TERRACES IN THE CAVITY

NT = 0 LT = 1.00&-6 HT = 1.00&-8

THERMAL RESISTANCE OF THE CONTACT

TETAC = 3.029

THRESHOLD VALUES OF THE LASER PARAMETERS

THRESHOLD CURRENT DENSITY (A/(cm↑2)	JTH	= 2.094518&3
GAIN THRESHOLD CURRENT DENSITY	JTHG	= 2.094497&3
ELECTRON LEAKAGE CURRENT DENSITY	JE	= 1.815259&-2
HOLE LEAKAGE CURRENT DENSITY	JH	= 2.605859&-3

TEMPERATURE INCREASES IN THE CENTRE OF THE FOLLOWING LAYERS:

P - GAAS LAYER	TC - T0	= 10.13 K
PP - (ALGA)AS LAYER	TP - T0	= 12.28 K
A - (ALGA)AS ACTIVE LAYER	TA - T0	= 14.01 K
NN - (ALGA)AS LAYER	TN - T0	= 15.05 K
TRANSFER N - GAAS LAYER	TT - T0	= 16.17 K
N - GAAS SUBSTRATE	TS - T0	= 16.20 K

DENSITIES OF HEAT SOURCES IN W/(M↑3)

LAYER	DENSITY	PERCENTAGE OF THE TOTAL HEAT FLUX
C	3.883709&12	28.462
P	8.679787&9	0.064
A	5.863833&13	42.918
N	1.081801&9	0.012
T	7.771312&12	28.440
S	3.122262&8	0.105

FREE CARRIER CONCENTRATIONS IN THE ACTIVE LAYER (CM↑-3)

ELECTRONS	NFC = 2.479057&17
HOLES	PFC = 2.247906&18

LOSSES (IN CM↑-1)

THRESHOLD LOCAL GAIN GTH = 93

```
INTERNAL LOSSES                                       ALFAI  = 24
     SCATTERING LOSSES                                ALFAS  =  0
     COUPLING LOSSES                                  ALFAC  =  0
     FREE CARRIER ABSORPTION IN THE
          ACTIVE LAYER                                ALFAFC = 17
             DUE TO ACCOUSTIC PHONONS                 ALFAA  = 15
                 ELECTRONS                            ALFAEA =  0
                 HOLES                                ALFAHA = 14

             DUE TO OPTICAL PHONONS                   ALFAO  =  3
                 ELECTRONS                            ALFAEO =  0
                 HOLES                                ALFAHO =  2
     FREE CARRIER ABSORPTION DUE TO
             ELECTRONS                                ALFAE  =  1
             HOLES                                    ALFAH  = 17

LOSSES IN THE PASSIVE LAYERS                          ALFAOUT= 32
     IN THE NN LAYER                                  ALFAN  =  7
             DUE TO ACCOUSTIC PHONONS                 ALFANA =  4
             DUE TO OPTICAL PHONONS                   ALFANO =  3
     IN THE PP LAYER                                  ALFAP  = 56
             DUE TO ACCOUSTIC PHONONS                 ALFAPA = 50
             DUE TO OPTICAL PHONONS                   ALFAPO =  6


EFFICIENCIES

INTERNAL QUANTUM EFFICIENCY OF THE
     SPONTANEOUS EMISSION                        ETASP = 0.8573
INTERNAL QUANTUM EFFICIENCY OF THE LASING        ETAI  = 0.6344
EXTERNAL DIFFERENTIAL QUANTUM EFFICIENCY
     OF THE LASING                               ETAD  = 0.3457


LIFETIMES (IN NSEC)
     RADIATIVE                                   TAUR  =  1.853
     NONRADIATIVE                                TAUNR = 11.127


DIFFUSION LENGTHS (IN MICRONS)

ELECTRON DIFFUSION LENGTH IN THE PP LAYER        LE = 1.755
HOLE DIFFUSION LENGTH IN THE NN LAYER            LH = 1.171


INDICES OF REFRACTION

     OF THE ACTIVE LAYER MATERIAL                NRA = 3.61993
     OF THE CONFINEMENT LAYER MATERIAL           NRB = 3.41514


CONFINEMENT FACTOR                               GAMMA = 0.55972


BEAM DIVERGENCE (ANGLE AT 0.5 OF THE FAR-FIELD INTENSITY
     DISTRIBUTION)

     IN RADIANS            TETA = 0.8454
     IN DEGRES             TETA = 48.44
```

18. Conclusions

The presented model enables us to carry out the optimization of the structure of the double-heterostructure GaAs/(AlGa)As diode laser with the point of view of the most important for us its properties, e.g., minimal threshold current density, minimal temperature sensitivity of its operation characteristics or minimal beam divergence. The optimization may be performed with the aid of the simple trial-and-error method or with a more sophisticated method of calculations, every time, however, using the self-consistent method.

The author would like once more to remind the reader, that most of the formulae presented in the model concern an ideal structure of the laser, e.g., homogeneous layers without defects, perfect ohmic contacts, a solder layer without voids etc.etc. Therefore, when the specified laser structure is considered, then in order to improve the exactness of the calculations the literature data should be replaced by the greatest possible numbers of experimental data obtained for this specified structure.

References

[1] CASEY H. C., Jr, STERN F., J. Appl. Phys. **47** (1976), 631.
[2] NELSON R. J., SOBERS R. G., J. Appl. Phys. **49** (1978), 6103.
[3] GARBUZOV D. N., [In] *Semiconductor Optoelectronics*, [Ed.] M.A. Herman, PWN, Warszawa 1980, p. 305.
[4] GARBUZOV D. N., KHALFIN V. B., TRUKAN M. K., AGATONOV V. G., ABDULLAEV A., Fiz. Tekh. Poluprovod. **12** (1978), 1368 (in Russian).
[5] CASEY H. C., Jr, PANISH M. B., *Heterostructure Lasers, Part A: Fundamental Principles*, Academic Press, New York 1978.
[6] ETTENBERG M., KRESSEL H., J. Appl. Phys. **47** (1976), 1538.
[7] HAKKI B. W., J. Appl. Phys. **42** (1971), 4981.
[8] KRESSEL H., BUTLER J. K., *Semiconductor Lasers and Heterojunction LEDs*, Academic Press, New York 1977, p. 419.
[9] Reference 8, p. 506.
[10] KRESSEL H., J. Electron. Mater. **4** (1975), 1081.
[11] KRESSEL H., ETTENBERG M., WITTKE J. P., LADANY I., [In] *Semiconductor Devices for Optical Communications*, Springer-Verlag, Berlin 1980, p. 9.
[12] NELSON R. J., SOBERS R. G., Appl. Phys. Lett. **32** (1978), 761.
[13] 't HOOFT G. V., VAN OPDORP C., Appl. Phys. Lett. **42** (1983), 813.
[14] DRISCOLL C. M. H., WILLOUGHBY A. F. W., MULLIN J. B., STRAUGHAN B. W., *Gallium Arsenide and Related Compounds*, Institute of Physics, London 1975, p. 275.
[15] CASEY H. C., Jr, PANISH M. B., *Heterostructure Lasers, Part B: Materials and Operating Characteristics*, Academic Press, New York 1978, Table 5.2.1.
[16] PIERRON E. D. PARKER D. L., MCNELY J. B., Acta Cryst. **21** (1966), 290.
[17] ETTENBERG M., PAFF R. J., J. Appl. Phys. **41** (1970), 3926.
[18] HENSHALL G. D., Appl. Phys. Lett. **31** (1977), 205.
[19] BIARD J. R., GARR W. N., REED B. S., Trans. AIME **230** (1964), 286.
[20] NASH F. R., HARTMAN R.L., J. Appl. Phys. **50** (1979), 3133.
[21] CARSLAW H. S., JAEGER J. C., *Conduction of Heat in Solids*, University Press, Oxford 1959, p. 265.
[22] KOBAYASHI T., FURUKAWA Y., Jpn. J. Appl. Phys. **14** (1975), 1981.
[23] NAKWASKI W., Kvantovaya Elektronika **6** (1979) 2609 (in Russian).
[24] BLAKEMORE J. S., J. Appl. Phys. **53** (1982), R123.

[25] Sze S. M., Irvin J. C., Solid State Electron. **11** (1968), 599.
[26] Stringfellow G. B., J. Appl Phys. **50** (1979), 4178.
[27] Neumann H., [In] *Semiconductor Sources of Electromagnetic Radiation*, [Ed.] M. A. Herman, PWN, Warszawa 1976, p. 45.
[28] Afromowitz M. A., J. Appl Phys. **44** (1973), 1292.
[29] Maycock P. D., Solid State Electron. **10** (1967), 161.
[30] Adachi S., J. Appl. Phys. **54** (1983), 1844.
[31] Amith A., Kudman I., Steigmeier E. F., Phys. Rev. **138** (1965), A1270.
[32] Garel-Jones P., Dyment J. C., IEEE J. Quantum Electron. **QE-11** (1975), 408.
[33] Botez D., RCA Review **39** (1978), 577.
[34] Botez D., Ettenberg M., IEEE J. Quantum Electron. **QE-14** (1978), 827.
[35] Pinkas E., Miller B. I., Hayashi I., Foy P. W., J. Appl. Phys. **43** (1972), 2827.
[36] Kressel H., Butler J. K., Hawrylo F. Z., Lockwood H. F., Ettenberg M., RCA Review **32** (1971), 393.
[37] Reference [8], Figure 7.4.6.

Received March 30, 1989
in revised form May 17, 1989

Имитация предусматриваемых эксплуатационных характеристик ширококонтактных лазерных диодов (AlGa)As с двойной гетероструктурой. III. Квантовые эффективности и тепловые свойства

Настоящая работа является третьей частью модели ширококонтактного лазерного диода (AlGa)As с двойной гетероструктурой. Представленные здесь формулы способствуют определению квантовых эффективностей лазерного диода и роста температуры диода.